Autochthonous tumors driven by *Rb1* loss have an ongoing requirement for the RBP2 histone demethylase

Samuel K. McBrayer[a], Benjamin A. Olenchock[a,b,c], Gabriel J. DiNatale[a], Diana D. Shi[a], Januka Khanal[a], Rebecca B. Jennings[a,d], Jesse S. Novak[a,d], Matthew G. Oser[a], Alissa K. Robbins[a], Rebecca Modiste[e], Dennis Bonal[e], Javid Moslehi[f], Roderick T. Bronson[g], Donna Neuberg[h], Quang-De Nguyen[e], Sabina Signoretti[a,d], Julie-Aurore Losman[a], and William G. Kaelin Jr.[a,i,1]

[a]Department of Medical Oncology, Dana-Farber Cancer Institute, Harvard Medical School, Boston, MA 02215; [b]Koch Institute for Integrative Cancer Research, Massachusetts Institute of Technology, Cambridge, MA 02142; [c]Division of Cardiovascular Medicine, Department of Medicine, Brigham and Women's Hospital, Harvard Medical School, Boston, MA 02115; [d]Department of Pathology, Brigham and Women's Hospital, Harvard Medical School, Boston, MA 02115; [e]Lurie Family Imaging Center, Center for Biomedical Imaging in Oncology, Dana-Farber Cancer Institute, Boston, MA 02210; [f]Division of Cardiovascular Medicine, Department of Medicine, School of Medicine, Vanderbilt University, Nashville, TN 37235; [g]Division of Immunology, Department of Microbiology and Immunobiology, Harvard Medical School, Boston, MA 02215; [h]Department of Biostatistics and Computational Biology, Dana-Farber Cancer Institute, Boston, MA 02215; and [i]Howard Hughes Medical Institute, Chevy Chase, MD 20815

Contributed by William G. Kaelin Jr., March 15, 2018 (sent for review September 12, 2017; reviewed by Jeff Settleman and David Tuveson)

Inactivation of the retinoblastoma gene (*RB1*) product, pRB, is common in many human cancers. Targeting downstream effectors of pRB that are central to tumorigenesis is a promising strategy to block the growth of tumors harboring loss-of-function *RB1* mutations. One such effector is retinoblastoma-binding protein 2 (RBP2, also called JARID1A or KDM5A), which encodes an H3K4 demethylase. Binding of pRB to RBP2 has been linked to the ability of pRB to promote senescence and differentiation. Importantly, genetic ablation of RBP2 is sufficient to phenocopy pRB's ability to induce these cellular changes in cell culture experiments. Moreover, germline *Rbp2* deletion significantly impedes tumorigenesis in *Rb1*$^{+/-}$ mice. The value of RBP2 as a therapeutic target in cancer, however, hinges on whether loss of RBP2 could block the growth of established tumors as opposed to simply delaying their onset. Here we show that conditional, systemic ablation of RBP2 in tumor-bearing *Rb1*$^{+/-}$ mice is sufficient to slow tumor growth and significantly extend survival without causing obvious toxicity to the host. These findings show that established *Rb1*-null tumors require RBP2 for growth and further credential RBP2 as a therapeutic target in human cancers driven by *RB1* inactivation.

genetically engineered mouse models | cancer | KDM5A | epigenetics | JARID1A

The pRB tumor suppressor protein, which is encoded by retinoblastoma gene *RB1*, governs diverse cellular processes and cell fate decisions (1), including cell cycle progression (2–4), differentiation (5–8), and senescence (9, 10), that together serve to prevent aberrant cell-autonomous growth and division. pRB function is suppressed via direct phosphorylation by cyclin-dependent kinases (CDK) (11) and stimulated by endogenous CDK inhibitors (CDK_i). Many human tumors have mutually exclusive mutations of *RB1* or the genes encoding these upstream regulators, leading to a loss of pRB tumor suppressor activity. Biallelic loss-of-function *RB1* mutations are the signature event in retinoblastomas and are also observed in virtually all small cell lung cancers (12) as well as a significant fraction of prostate, breast, and bladder cancers (1). Retinoblastomas and small cell lung cancers are neuroendocrine tumors and loss of pRB has also been linked to the acquisition of neuroendocrine features in non-small cell lung cancer (13–15) and prostate cancer (16). Interestingly, *Rb1*$^{+/-}$ mice spontaneously develop neuroendocrine tumors of the prostate and thyroid glands (17, 18).

The canonical function of pRB relates to its ability to bind to members of the E2F transcription factor family. pRB/E2F complexes actively repress the transcription of genes required for cell-cycle progression, especially at the G1/S transition. pRB also binds to the RBP2 H3K4 demethylase and, in so doing, promotes differentiation and senescence in certain models (19). RBP2, unfettered by pRB, prevents senescence and differentiation (20), stimulates invasion and metastasis (21, 22), and promotes drug resistance (23).

Germline inactivation of *Rbp2* is tolerated in mice on a mixed genetic background (24). Given the mounting evidence that RBP2 functions as an oncogene, we previously crossed such mice with *Rb1*$^{+/-}$ mice (20). Remarkably, loss of even one *Rbp2* allele significantly delayed the onset of pituitary and thyroid tumors in *Rb1*$^{+/-}$ mice and a significant fraction of *Rb1*$^{+/-}$ mice lacking both *Rbp2* alleles did not develop overt tumors and had normal lifespans.

Significance

Developing therapeutic strategies for tumors driven by tumor suppressor gene inactivation, as opposed to oncogene activation, represents a significant challenge in oncology. While restoration of tumor suppressor functionality is generally not feasible, inhibiting proteins that act downstream of lost tumor suppressors represents one strategy to overcome this challenge. In this study, we applied this concept to the tumor suppressor gene *retinoblastoma 1* (*RB1*). The *RB1* gene product, pRB, associates with the RBP2 histone demethylase and RBP2 is deregulated in *RB1*-null cancers. Here, we show that genetic ablation of RBP2 in established, autochthonous pRB-defective murine tumors retards their growth and enhances mouse survival. Our findings provide a further rationale for the development and testing of pharmacological RBP2 inhibitors for cancer treatment.

Author contributions: S.K.M., J.-A.L., and W.G.K. designed research; S.K.M., B.A.O., G.J.D., D.D.S., J.K., R.B.J., J.S.N., M.G.O., A.K.R., R.M., D.B., and J.M. performed research; S.K.M. contributed new reagents/analytic tools; S.K.M., B.A.O., D.D.S., R.B.J., J.S.N., J.M., R.T.B., D.N., Q.-D.N., S.S., J.-A.L., and W.G.K. analyzed data; and S.K.M. and W.G.K. wrote the paper.

Reviewers: J.S., Calico Life Sciences; and D.T., Cold Spring Harbor Laboratory.

The authors declare no conflict of interest.

[1]To whom correspondence should be addressed. Email: william_kaelin@dfci.harvard.edu.

This article contains supporting information online at www.pnas.org/lookup/suppl/doi:10.1073/pnas.1716029115/-/DCSupplemental.

Published online April 2, 2018.

This study did not address, however, the requirement for RBP2 in tumor maintenance as opposed to tumor initiation. This distinction is clearly critical with respect to the likelihood that pharmacologically inhibiting RBP2 will lead to therapeutic outcomes in patients with pRB-defective cancers. To this end, we used *Rb1*$^{+/-}$ mice carrying conditional *Rbp2* alleles and a transgene encoding the tamoxifen-inducible recombinase Cre–ER to test the effects of RBP2 ablation on the growth of autochthonous pituitary and thyroid tumors arising in these mice. Furthermore, we assessed whether acute systemic RBP2 inactivation in adult mice causes toxicity in normal tissues, with a particular focus on potential implications for cardiac function, given earlier studies linking RBP2 and altered H3K4 methylation to congenital cardiac defects (25).

Results

To test the effects of genetic RBP2 ablation on tumor growth and maintenance in *Rb1*$^{+/-}$ mice, we used a previously described conditional *Rbp2* allele that features loxP sites flanking exons 5 and 6 that permits *Rbp2* inactivation after Cre recombinase-mediated recombination (24). We first designed qPCR assays to distinguish the null and conditional *Rbp2* alleles so that we could assess recombination efficiencies for this locus in various tissues and validated that these assays were specific and quantitative using predefined mixtures of genomic DNA isolated from mouse embryonic fibroblasts (MEFs) derived from *Rbp2*$^{lox/lox}$ mice that did or did not express Cre recombinase during embryogenesis (Fig. S1 *A* and *B*).

Next, through appropriate matings, we created *Rbp2*$^{lox/lox}$; *Cre–ER* mice on a C57BL/6 background that ubiquitously express a Cre–ER fusion protein that can be activated by administration of tamoxifen. We then treated them with tamoxifen daily by oral gavage for 5 d and euthanized them 6 d later (26). Mice lacking the Cre–ER fusion or treated with vehicle rather than tamoxifen were tested in parallel as negative controls. Tamoxifen treatment caused nearly complete conversion of the conditional *Rbp2* allele to the null allele in a Cre–ER-dependent manner in glands that give rise to tumors in *Rb1*$^{+/-}$ mice (pituitary and thyroid, Fig. 1 *A–D*) and in other tissues, including the heart (Fig. S1 *C* and *D*). Conversion of the conditional *Rbp2* allele to the null allele corresponded with suppression of RBP2 protein expression in both pituitary and heart tissues (Fig. 1*E* and Fig. S1*E*). Thus, our experimental approach enables inducible, near-complete *Rbp2* deletion in diverse tissues in adult mice within a timeframe of 2 wk.

Rbp2$^{-/-}$ mice on a pure C57BL/6 background die perinatally, associated with cardiac septal defects, while mice on a mixed background are viable, born at the expected Mendelian ratios, and have no gross phenotypes (24), suggesting that much of the toxicity of RBP2 loss is related to strain-specific effects in purebred mice. However, the phenotypes of such germline knockouts can be confounded by developmental compensation by paralogous genes and do not necessarily predict the consequences of acute gene inactivation in somatic adult tissues. In this regard, *Rbp2* has several paralogs, including *Kdm5b*, *Kdm5c*, and *Kdm5d*, which encode the demethylases PLU-1, SMCX, and SMCY, respectively. Moreover, pituitary tumors that arise in *Rbp2*$^{-/-}$; *Rb1*$^{+/-}$ mice display elevated expression of PLU-1, providing a precedent for compensation by other H3K4 histone demethylases (20). To evaluate the safety of systemic, acute RBP2 suppression in adult mice, we measured the weights of *Rbp2*$^{lox/lox}$; *Cre–ER* mice as a surrogate for gross toxicity following tamoxifen administration. Mice treated with tamoxifen showed no significant decline in body weight over a 30-d period relative to pretreatment measurements or compared with corn oil-treated mice that served as controls, suggesting that acute *Rbp2* deletion is well tolerated in adult mice (Fig. S2*A*).

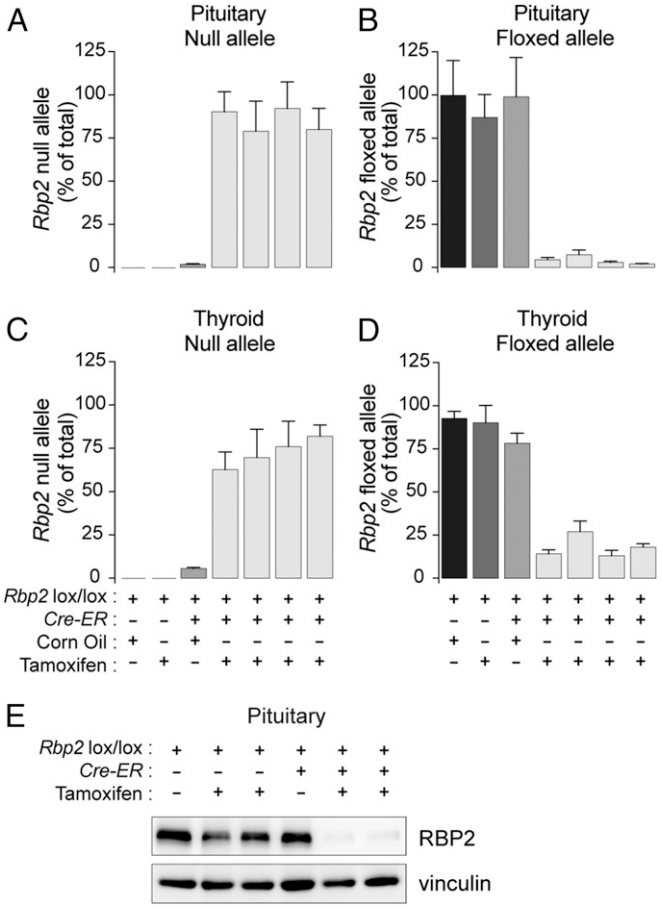

Fig. 1. Inducible deletion of *Rbp2* in vivo. (*A–D*) qPCR-based allelic frequency assays for the Rbp2 null allele in normal pituitary (*A*) and thyroid tissues (*C*) and for the Rbp2 floxed allele in normal pituitary (*B*) and thyroid tissues (*D*) from *Rbp2*$^{lox/lox}$ and *Rbp2*$^{lox/lox}$; *Cre–ER* mice. Mice were treated with tamoxifen or corn oil by oral gavage daily for 5 consecutive days. Pituitary and thyroid glands were harvested for gDNA extraction 10 d after the first dose. (*E*) RBP2 immunoblot in pituitary tissues harvested from *Rbp2*$^{lox/lox}$ and *Rbp2*$^{lox/lox}$; Cre–ER mice. Mice were treated with tamoxifen or corn oil and tissues were harvested as in *A–D*. For *A–D*, $n \geq 3$ and data presented are means ± SD.

We specifically evaluated cardiac function in tamoxifen-treated *Rbp2*$^{lox/lox}$; *Cre–ER* mice, given the cardiac septal defects observed in some *Rbp2*$^{-/-}$ mice on a C57BL/6 genetic background (24) and a recent study linking mutations in histone-modifying genes, including *RBP2* and *KDM5B*, with congenital heart disease (25). Echocardiography revealed no changes in ejection fraction (EF) or fractional shortening (FS) of the hearts of tamoxifen-treated animals versus oil-treated controls and histological examination of heart tissues showed no gross morphological differences between the two cohorts (Fig. S2 *B–D* and Movies S1 and S2). We also examined whether acute, whole-body *Rbp2* deletion induces renal, hepatic, or hematologic toxicities. We first surveyed various tissues and found that RBP2 expression was ablated in brain tissue (Fig. S3*A*) and white blood cells (WBCs) (Fig. S4*A*) in tamoxifen-treated *Rbp2*$^{lox/lox}$; *Cre–ER* mice compared with tamoxifen-treated *Rbp2*$^{lox/lox}$ controls, whereas baseline RBP2 expression was undetectable in mouse liver and kidney (Fig. S3*B*). Serum chemistry and complete blood count (CBC) analyses did not reveal signs of toxicity following *Rbp2* deletion with the exception of modest, nominally statistically significant decreases in serum cholesterol and total WBCs (Figs. S3*C* and S4*B*). Importantly, platelet counts were

not significantly reduced and WBC counts did not drop below the reported normal range for mice, indicating that *Rbp2* deletion does not cause significant bone marrow suppression. Taken together, these data demonstrate that acute RBP2 suppression is not grossly toxic to adult mice.

To test the effects of RBP2 ablation on the growth of established tumors driven by *Rb1* inactivation, we created mice, through appropriate breedings, that were $Rbp2^{lox/lox}$; $Rb1^{+/-}$; *Cre–ER* or $Rbp2^{+/+}$; $Rb1^{+/-}$; *Cre–ER* and monitored their pituitary and thyroid tumor development by monthly MRI that began when they were 5 mo old (Fig. 2). Once tumors were detected, the mice were given five consecutive daily doses of tamoxifen to activate Cre–ER and selectively delete *Rbp2* in the $Rbp2^{lox/lox}$ cohort. The $Rbp2^{+/+}$; $Rb1^{+/-}$; *Cre–ER* mice served as important controls for nonspecific effects related to Cre activation, which can induce a DNA damage response, and other tamoxifen effects unrelated to Cre activation. Importantly, no significant differences were observed between the two cohorts with respect to age or tumor size at the time tamoxifen treatment was initiated (Fig. S5 *A*, *E*, and *F*). Ratios of males to females deviated slightly from 1:1 in both cohorts, with a higher ratio seen in the $Rbp2^{lox/lox}$ cohort relative to the $Rbp2^{+/+}$ cohort (Fig. S5*B*), although this difference was not statistically significant ($P = 0.37$). For most of the mice the first tumor detected, and hence the indication for tamoxifen, was a thyroid tumor with or without a concurrent pituitary tumor. More $Rbp2^{+/+}$ mice had pituitary tumors at tamoxifen initiation compared with the $Rbp2^{lox/lox}$ cohort (10 versus 6 mice, respectively) and fewer $Rbp2^{+/+}$ mice had thyroid tumors at enrollment relative to the $Rbp2^{lox/lox}$ cohort (15 versus 19 mice, respectively) (Fig. S5 *C* and *D*). After the initial 5 d of tamoxifen therapy mice continued to receive tamoxifen doses once per week for the remainder of the study in an effort to prevent emergence of RBP2-positive tumor cells in the $Rbp2^{lox/lox}$ cohort. Mice underwent MRI at 2, 4, 6, 10, and 14 wk after enrollment to quantify tumor volume. Mice were monitored frequently and euthanized when they appeared moribund, distressed, or lost more than 25% of their body weight. Endpoints for the study included tumor growth and survival.

Genetic ablation of RBP2 in thyroid tumors potently attenuated tumor growth and, in a few cases, induced dramatic tumor regression (Fig. 3*B*). In the $Rbp2^{+/+}$ cohort, 10 of 14 mice displayed steadily increasing tumor burden, as quantified by MRI, with volumes surpassing 30 mm^3 in the 14 wk following tamoxifen treatment, albeit with wide variation in the growth rates of individual tumors (Fig. 3 *A* and *C*). In contrast, tamoxifen treatment strongly suppressed tumor growth in 11 of 17 $Rbp2^{lox/lox}$ mice ("responders"), with only 6 of 17 mice displaying thyroid tumor burden volumes exceeding 30 mm^3 ("nonresponders") over the same time period (Fig. 3 *B* and *D*). Five of the 17 thyroid tumors in the $Rbp2^{lox/lox}$ mice grew rapidly and surpassed 80 mm^3 in volume over the course of 14 wk. In subsequent immunohistochemistry (IHC) analyses, we found that two of these five tumors displayed residual RBP2 expression (Fig. S8) that likely accounts for their rapid growth. In the three remaining tumors, we found that RBP2 expression was completely abolished, implying these tumors were truly resistant to RBP2 loss. Between 2 and 14 wk after treatment, multiple $Rbp2^{lox/lox}$ mice displayed substantial thyroid tumor shrinkage, including one tumor that nearly completely resolved by week 10 (Fig. 3*B*, *Lower*). Altogether, there was a significant difference in thyroid tumor growth kinetics between the $Rbp2^{+/+}$ and $Rbp2^{lox/lox}$ cohorts, translating to an approximately sixfold reduction in median tumor volume 14 wk after treatment initiation in the latter group of mice relative to the former (Fig. 3*E*).

Although fewer mice were enrolled in the study bearing pituitary tumors compared with thyroid tumors, a clear trend was observed between RBP2 loss and pituitary tumor inhibition. In the $Rbp2^{+/+}$ cohort, six of eight mice (75%) showed evidence of continued pituitary tumor growth in the weeks following tamoxifen treatment and harbored tumors surpassing 30 mm^3 in volume at the final imaging time point. A similar pattern was seen in only two of five mice (40%) in the $Rbp2^{lox/lox}$ cohort (Fig. 4 *A*–*D*). In contrast to thyroid tumors, pituitary tumors did not significantly regress in $Rbp2^{lox/lox}$ mice. Rather, three of five mice in this cohort showed disease stabilization in the 10 wk following tamoxifen treatment. There was a clear trend toward decreased pituitary tumor growth rates in $Rbp2^{lox/lox}$ mice compared with $Rbp2^{+/+}$ mice, resulting in decreased median tumor volumes from 4 to 14 wk after induction of tamoxifen treatment. This effect approached but did not reach statistical significance ($P = 0.114$), presumably because of the low number of mice with measurable pituitary tumors at the time of study enrollment (Fig. 4*E*). The antitumor effects of RBP2 ablation described above translated to significantly longer survival of $Rbp2^{lox/lox}$; $Rb1^{+/-}$; *Cre–ER* mice relative to $Rbp2^{+/+}$; $Rb1^{+/-}$; *Cre–ER* mice following tamoxifen treatment (Fig. 5*A*). Median overall survival times in the $Rbp2^{+/+}$ and $Rbp2^{lox/lox}$ cohorts were 108 d and 153 d, respectively, an increase of more than 40% in the latter group. Interestingly, RBP2 ablation appeared to prolong survival in tumor-bearing female mice to a greater extent than in tumor-bearing male mice (Fig. S6).

We considered the possibility that the effects of RBP2 inactivation on tumor growth might be diluted if a considerable number of tumor cells escaped *Rbp2* recombination and dominated the tumors over time. To address this, we assayed RBP2 expression in tumor samples derived from mice at the time of euthanizing by IHC. First, we confirmed that our IHC assay was specific for RBP2 by testing normal pituitary and brain tissue samples harvested from tamoxifen-treated $Rbp2^{lox/lox}$ and $Rbp2^{lox/lox}$; *Cre–ER* mice. Consistent with previous tissue immunoblots (Fig. 1*E* and Fig. S3*A*), IHC analysis revealed nearly complete loss of RBP2 expression in both normal pituitary and brain tissues derived from $Rbp2^{lox/lox}$; *Cre–ER* mice, but not $Rbp2^{lox/lox}$ controls (Fig. S7). Importantly, RBP2 IHC in $Rbp2^{lox/lox}$; $Rb1^{+/-}$; *Cre–ER* and $Rbp2^{+/+}$; $Rb1^{+/-}$; *Cre–ER* tumor tissue samples showed that potent RBP2 suppression was observed in pituitary and thyroid tumors in 13 of 15 $Rbp2^{lox/lox}$ mice at the time of euthanizing (Fig. 5*B*). However, two thyroid tumors from nonresponder mice displayed persistent RBP2 expression in a fraction of tumor cells (Fig. S8). Residual RBP2 expression was not observed in thyroid tumors from responder mice (Fig. S8), suggesting that incomplete *Rbp2* recombination may have

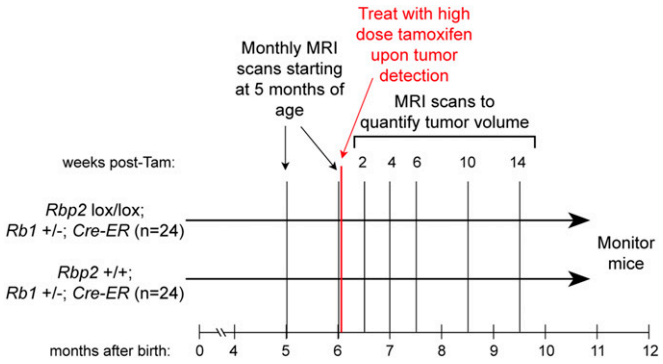

Fig. 2. Schema of experimental design for inducible deletion of *Rbp2* in tumors of $Rb1^{+/-}$ mice. C57BL/6 mice of the indicated genotypes began monthly MRI at 5 mo of age to detect the development of pituitary and thyroid tumors. Once tumors were detected, the mice were administered tamoxifen (Tam) by oral gavage on 5 consecutive days. MRI scans were performed 2, 4, 6, 10, and 14 wk after initiation of tamoxifen treatment to quantify tumor volume. Additional doses of tamoxifen were given once per week until mice were euthanized due to tumor burden.

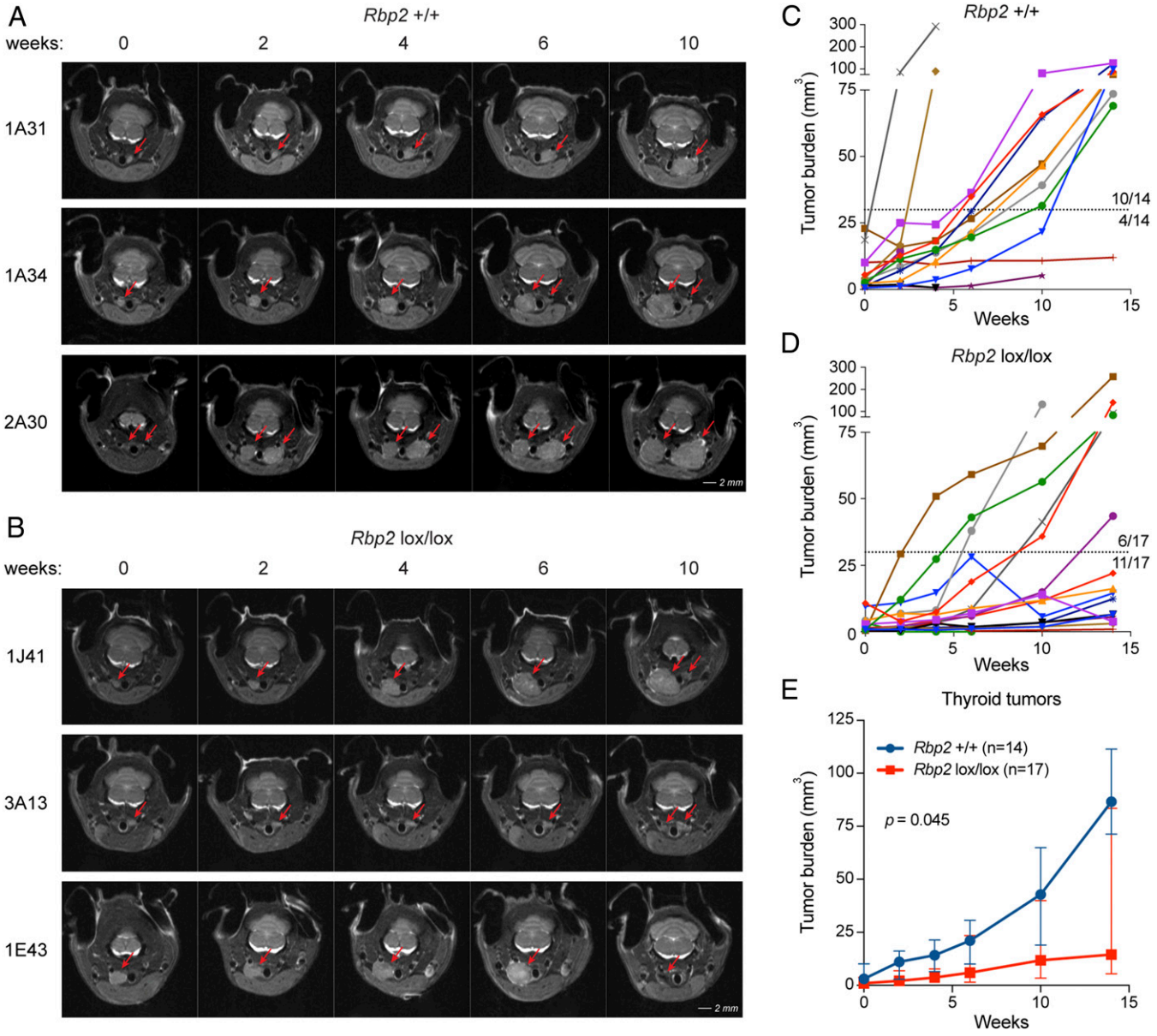

Fig. 3. *Rbp2* deletion retards the growth of established *Rb1*-null thyroid tumors. (*A* and *B*) Representative MRIs of thyroid tumors in $Rbp2^{+/+}$; $Rb1^{+/-}$; *Cre–ER* (*A*) and $Rbp2^{lox/lox}$; $Rb1^{+/-}$; *Cre–ER* (*B*) mice before (0 wk) and 2, 4, 6, and 10 wk after initiation of tamoxifen treatment as outlined in Fig. 2. Red arrows indicate tumors. (Scale bar: 2 mm.) Imaging results from three mice in each cohort are shown and their unique study IDs are listed at *Left*. In *A*, all three mice had progressive disease. In *B*, mouse 1J41 had progressive tumor growth, 3A13 had stable disease, and 1E43 had a regression at week 10. (*C* and *D*) Thyroid tumor burden in $Rbp2^{+/+}$; $Rb1^{+/-}$; *Cre–ER* (*C*) and $Rbp2^{lox/lox}$; $Rb1^{+/-}$; *Cre–ER* (*D*) mice before and 2, 4, 6, 10, and 14 wk after initiation of tamoxifen treatment as quantified by MRI. Colored lines represent individual mice. Dashed line indicates 30 mm^3 tumor burden and the fraction of mice surpassing and failing to exceed this threshold is listed for each cohort. Two mice in the $Rbp2^{+/+}$ cohort had both left and right thyroid tumors at the time of enrollment. In these mice, tumor burden was calculated by summing the volumes of the two tumors at each time point. (*E*) Median thyroid tumor burden over time in $Rbp2^{+/+}$ and $Rbp2^{lox/lox}$ cohorts represented in *C* and *D*. Error bars indicate interquartile range. *P* value was determined by a mean-based longitudinal mixed-effects model to accommodate repeated measurements within animals.

compromised the antitumor response to RBP2 ablation in a subset of the mice and caused an underestimation of the survival benefit associated with this intervention. We also confirmed loss of pRB expression in tumors (Fig. 5*B*) relative to normal pituitary and thyroid tissues (Fig. S9), thereby validating previous studies linking *Rb1* loss of heterozygosity to tumorigenesis in $Rb1^{+/-}$ mice (17, 18).

To ask whether RBP2 ablation causes global up-regulation of H3K4me3 marks, we performed IHC analysis of thyroid tumors collected from tamoxifen-treated $Rbp2^{lox/lox}$; $Rb1^{+/-}$; *Cre–ER* and $Rbp2^{+/+}$; $Rb1^{+/-}$; *Cre–ER* mice at the time of euthanizing. Interestingly, H3K4me3 levels were dramatically induced by RBP2 ablation in the responder mice but were unaffected in nonresponder mice relative to *Rbp2* wild-type controls (Fig. 5 *C* and *D*). This failure to affect H3K4me3 tumor levels in nonresponder mice occurred even in tumors where RBP2 expression was undetectable, suggesting that resistance in some tumors was mediated by alternative regulators of H3K4 methylation. To begin to address the potential roles of RBP2 paralogs in this regard, we profiled expression of SMCX (encoded by *Kdm5c*) in the same series of tumors and found that levels of this histone demethylase were not induced by RBP2 ablation and were not

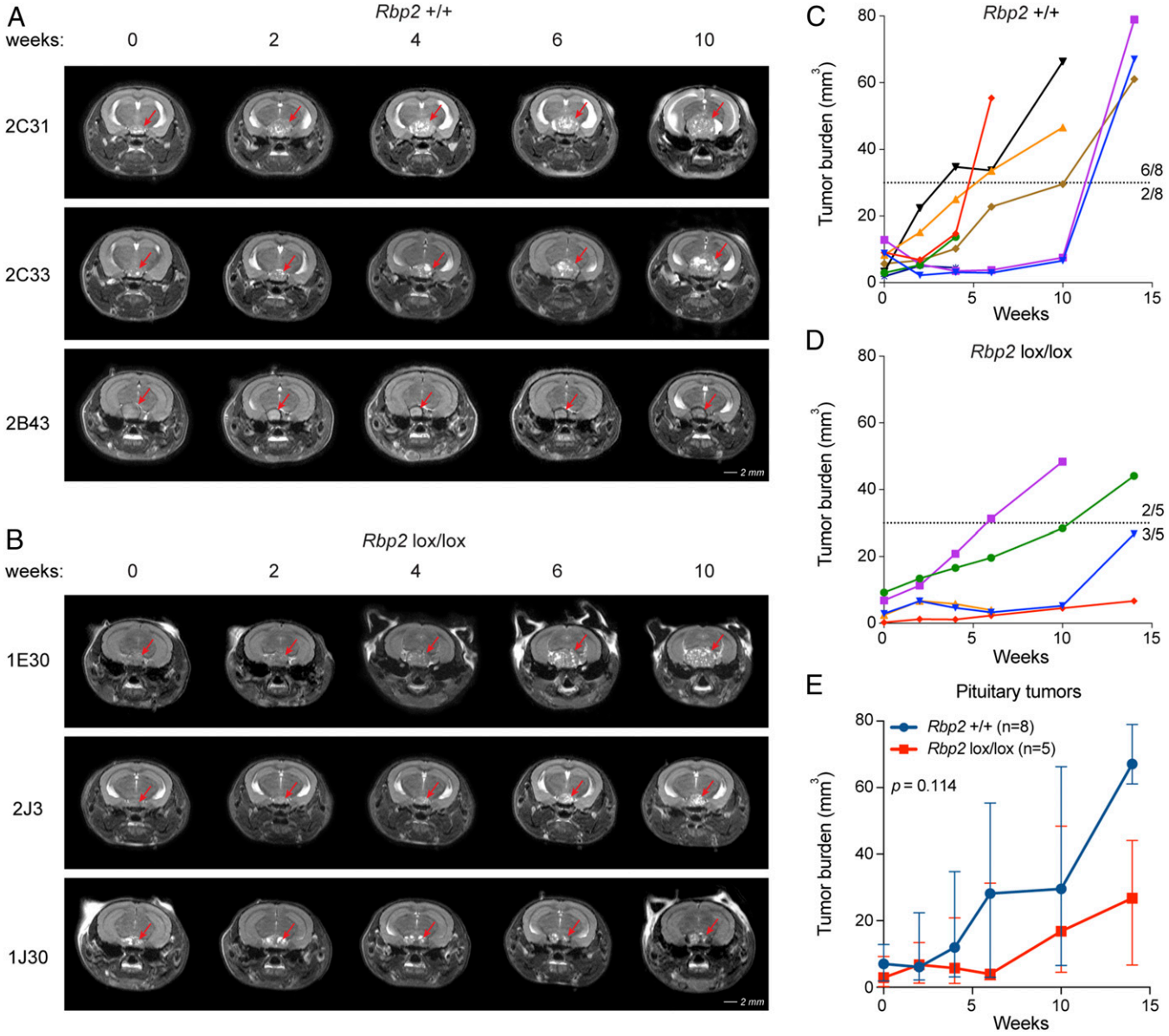

Fig. 4. *Rbp2* deletion retards the growth of established *Rb1*-null pituitary tumors. (*A* and *B*) Representative MRIs of pituitary tumors in $Rbp2^{+/+}$; $Rb1^{+/-}$; *Cre–ER* (*A*) and $Rbp2^{lox/lox}$; $Rb1^{+/-}$; *Cre–ER* (*B*) mice before (0 wk) and 2, 4, 6, and 10 wk after initiation of tamoxifen treatment as in Fig. 2. Red arrows indicate tumors. (Scale bar: 2 mm.) Imaging results from three mice in each cohort are shown and their unique study IDs are listed at *Left*. In *A*, mice 2C31 and 2C33 had progressive disease and mouse 2B43 had stable disease; in *B*, mouse 1E30 had progressive disease and mice 2J3 and 1J30 had stable disease. (*C* and *D*) Pituitary tumor burden in $Rbp2^{+/+}$; $Rb1^{+/-}$; *Cre–ER* (*C*) and $Rbp2^{lox/lox}$; $Rb1^{+/-}$; *Cre–ER* (*D*) mice before and 2, 4, 6, 10, and 14 wk after initiation of tamoxifen treatment as quantified by MRI. Colored lines represent individual mice. Dashed line indicates 30 mm^3 tumor burden and the fraction of mice surpassing and failing to exceed this threshold is listed for each cohort. (*E*) Median pituitary tumor burden over time in $Rbp2^{+/+}$ and $Rbp2^{lox/lox}$ cohorts represented in *C* and *D*. Error bars indicate interquartile range. *P* value was determined by a mean-based longitudinal mixed-effects model to accommodate repeated measurements within animals.

correlated with responder status. Unfortunately, we were unable to assess the expression of the RBP2 paralogs PLU-1 and SMCY by IHC with the reagents currently available to us.

Discussion

Prior studies showed that genetic suppression of RBP2 at the time of tumor cell initiation (20) or tumor cell implantation (22) could inhibit tumor growth, but did not address the therapeutically important question of whether there is an ongoing requirement for RBP2 in established tumors. In this study, we showed that RBP2 suppression exerts robust antitumor effects in established $Rb1^{-/-}$ thyroid and pituitary tumors in mice. Moreover, we found that acute, systemic RBP2 suppression does not cause gross toxicity or cardiac dysfunction in adult mice, suggesting that potent RBP2 inhibition will be safe in humans. Together, these findings should help galvanize ongoing efforts to discover drugs that inhibit RBP2 and develop them as potential anticancer agents.

There is mounting evidence that supports a critical role for RBP2 in a variety of tumors, including neuroendocrine tumors. For example, Maggi et al. (27) recently reported that RBP2 is overexpressed in neuroendocrine tumors of diverse origin and that siRNA-mediated inhibition of RBP2 suppressed the proliferation, migration, and invasion of pancreatic and lung

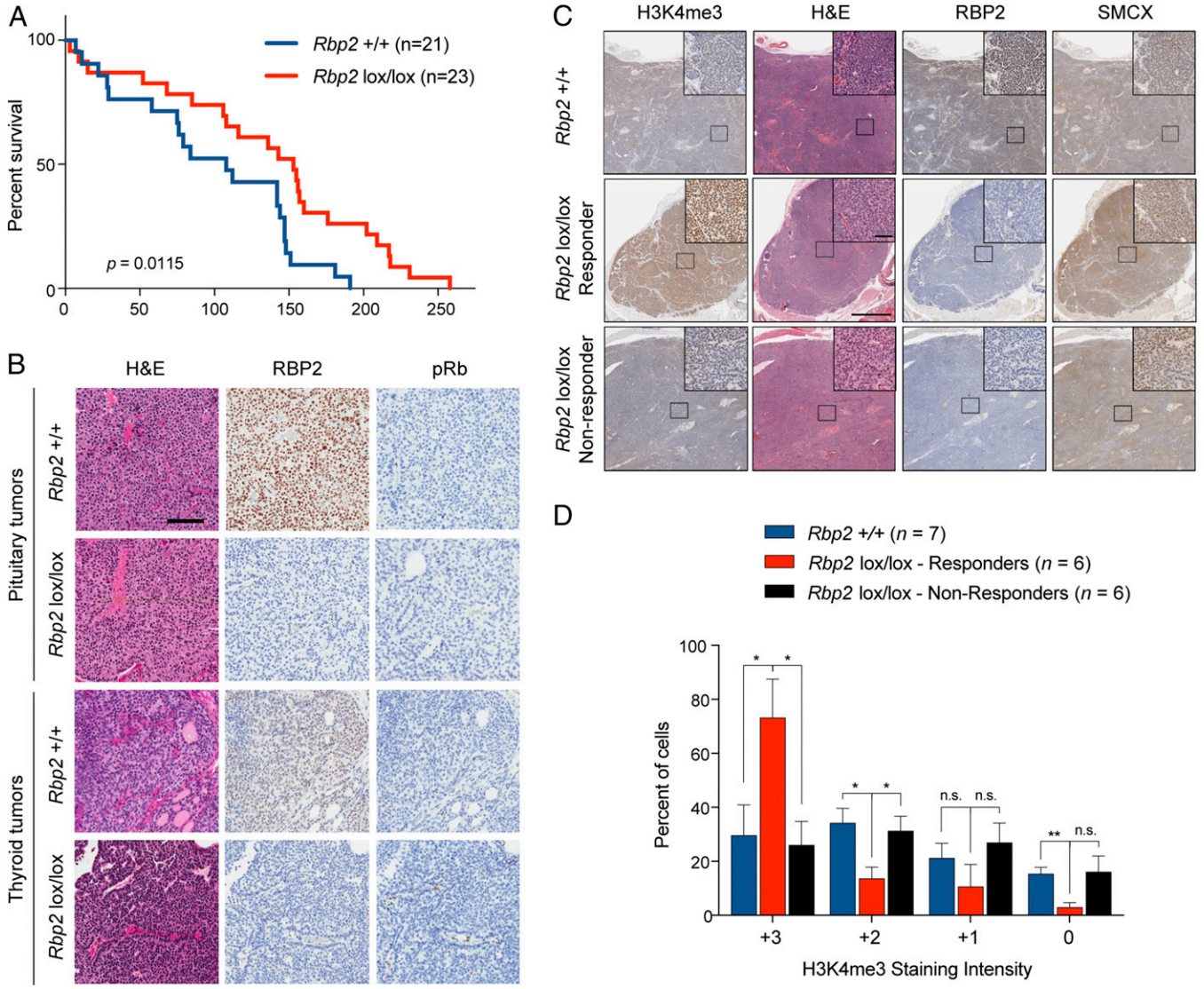

Fig. 5. *Rbp2* deletion in established tumors significantly extends survival of $Rb1^{+/-}$ mice. (*A*) Kaplan–Meier survival curves of $Rbp2^{+/+}$; $Rb1^{+/-}$; *Cre–ER* and $Rbp2^{lox/lox}$; $Rb1^{+/-}$; *Cre–ER* mice treated with tamoxifen as in Fig. 2, with day 0 being the first day of tamoxifen treatment. *P* value was determined by log-rank test. (*B*) Immunohistochemical analysis of pituitary and thyroid tumors obtained at necropsy in representative tamoxifen-treated $Rbp2^{+/+}$; $Rb1^{+/-}$; *Cre–ER* and $Rbp2^{lox/lox}$; $Rb1^{+/-}$; *Cre–ER* mice from the study in *A*. Serial tumor tissue sections from mice in the indicated cohorts were stained with hematoxylin and eosin (H&E) and RBP2 and pRB antibodies. (Scale bar: 100 μm.) (*C*) Immunohistochemical analysis of thyroid tumors obtained at necropsy in representative tamoxifen-treated $Rbp2^{+/+}$; $Rb1^{+/-}$; *Cre–ER* and $Rbp2^{lox/lox}$; $Rb1^{+/-}$; *Cre–ER* mice from the study in *A*. Responder status for mice from the $Rbp2^{lox/lox}$ cohort is indicated and based on tumor growth kinetics as depicted in Fig. 3*D*. Serial tumor tissue sections were stained with antibodies against RBP2, SMCX, and H3K4me3 or with H&E. (Scale bar: 1 mm, for 2× magnification main images.) (Scale bar: 50 μm, for 40× magnification *Insets*.) (*D*) Quantification of H3K4me3 staining intensity for a subset of the thyroid tumors from *A* analyzed as in *C*. Data presented are means ± SEM; $*P < 0.05$, $**P < 0.01$. Two-tailed *P* values were determined by unpaired *t* test. n.s., nonsignificant.

neuroendocrine cancer cell lines. Moreover, our group showed that germline inactivation of *Rbp2* caused a significant delay in the development of mouse neuroendocrine tumors linked to *Rb1* or *Men1* deletion (20).

RBP2 has also been reported to be overexpressed in non-small cell lung (22), gastric (28), and highly metastatic breast cancers (21). RBP2 suppression is sufficient to cause senescence in gastric cancer lines (28) and to decrease tumor cell metastasis to the lung in both xenograft and genetic models of breast cancer (21).

The functional interaction between pRB and RBP2 may indicate tumor contexts in which RBP2 inhibitors would be expected to display the greatest antitumor activity clinically. RBP2 was among the first proteins identified to bind to pRB (29–31) and early studies from our group and others suggested that the binding of pRB to RBP2 is linked to pRB's ability to promote senescence and, in some contexts, differentiation (19). Importantly, in cell culture models, loss of RBP2 is sufficient to phenocopy the ability of pRB to promote senescence when reintroduced into $RB1^{-/-}$ osteosarcoma cells (19) and the ability of pRB to cooperate with MyoD to promote myogenic differentiation of $Rb1^{-/-}$ mouse embryonic fibroblasts (20), coincident with an increase in H3K4 methylation. This suggests that pRB is an RBP2 antagonist, although transcriptional and DNA-binding studies suggest that the interaction between pRB and RBP2 is more nuanced (19). Nonetheless, pRB loss deregulates RBP2 and, therefore, patients with tumors harboring deletions or inactivating mutations in *RB1* would be predicted to be ideal candidates for treatment with RBP2 inhibitors. In

addition, many $RB1^{+/+}$ cancers harbor mutations, such as loss of p16 or amplification of cyclin D1, that promote phosphorylation of pRB, which disrupts the binding of pRB to RBP2. It is therefore possible that such tumors, which numerically are more common than $RB1^{-/-}$ tumors, would also be sensitive to RBP2 inhibitors.

Recently, multiple groups have developed a variety of chemically distinct pharmacological inhibitors of the KDM5 histone demethylase family (32–40), which includes RBP2, PLU-1, SMCX, and SMCY. Two inhibitors, YUKA1 and YUKA2, were developed to selectively inhibit RBP2 (32), whereas other inhibitors have been developed to more broadly target all KDM5 family members. One of these inhibitors, CPI-455, inhibits all four KDM5 family members with low nanomolar IC_{50} values in vitro and potently suppresses the emergence of drug-tolerant persister cancer cells following prolonged exposure to various anticancer signal transduction inhibitors (33), a process that has been shown to be KDM5 dependent (23, 41, 42).

It is not yet known whether it would be advantageous to specifically inhibit KDM5A or whether it would be more desirable to inhibit multiple KDM5 family members, given the possibility of functional redundancy among the paralogs. In this regard, PLU-1 promotes tumor growth in some models and is up-regulated in pituitary tumors in $Rb1^{+/-}$; $Rbp2^{-/-}$ mice (20), suggesting that it might compensate for RBP2 loss.

In an unplanned subgroup analysis, it appeared that the benefit of inactivating RBP2 was greater in tumor-bearing female mice compared with tumor-bearing male mice (Fig. S6). Although this finding clearly requires validation in an independent set of mice, it is striking, given that most thyroid tumors in humans occur in women. Moreover, it raises the intriguing possibility that *Kdm5d*, located on the Y chromosome, and *Kdm5c*, located on the X chromosome, differ in their ability to compensate for RBP2 loss.

One unresolved issue regarding RBP2 function that could ultimately determine the clinical utility of RBP2 inhibitors pertains to whether specific cellular phenotypes observed following RBP2 silencing can be specifically ascribed to loss of its catalytic activity. In addition to its canonical H3K4 demethylase activity, RBP2 also influences chromatin structure and gene expression through mechanisms that are independent of its demethylase activity. In cell culture models, RBP2's demethylase activity appears to be important for preventing senescence (20) and promoting the formation of drug persister cells (33). On the other hand, RBP2's ability to promote expression of the metastasis-associated gene *TNC* (encoding tenascin C) and to promote invasion of the metastatic LM2 breast cancer cell line is not attenuated by an RBP2 missense mutation, H483A, that abrogates RBP2's demethylase activity (21, 24). Likewise, overexpression of the RBP2 H483A mutant stimulates migration, invasion, and anchorage-independent growth of immortalized pancreatic islet cells in a manner indistinguishable from the wild-type protein (27). A caveat to such overexpression studies is that RBP2 contains the LXCXE motif that was first found in the SV40 large T, adenovirus E1A, and human papillomavirus E7 oncoproteins and might, accordingly, sequester a number of cellular proteins when overexpressed, including other members of the pRB family. If, however, critical oncogenic effects of RBP2 activation are confirmed to be independent of its catalytic activity, alternative therapeutic strategies designed to destabilize the enzyme may be required to realize the maximal antitumor response induced by RBP2 suppression.

Materials and Methods

Cell Culture. $Rbp2^{lox/lox}$ and $Rbp2^{-/-}$ MEFs were generated as previously described (20, 24). Cells were cultured in DMEM (Gibco, 11995–065) containing 10% FBS and 1% penicillin/streptomycin and maintained in the presence of 5% CO_2 at 37 °C.

***Rbp2* Allelic Frequency Assays.** Genomic DNA extraction from MEFs and tissue samples was done using the QIAmp DNA Blood Mini Kit (Qiagen, 51106) according to manufacturer instructions. Tissue samples were homogenized in PBS using a TissueLyser II (Qiagen).

Allelic frequency qPCR assays were designed to quantify *Rbp2* floxed and null alleles in genomic DNA samples based on the presence and absence of exons 5 and 6, respectively (24). A control qPCR assay designed to amplify a genomic DNA sequence common to both alleles (exon 4 and following intron of *Rbp2*) was used for normalization. Real-time qPCR was performed using RT^2 SYBR Green/ROX qPCR Master Mix (Qiagen). All calculations were performed using the $2^{-\Delta\Delta Ct}$ method. Standards containing mixtures of known quantities of gDNA derived from $Rbp2^{lox/lox}$ and $Rbp2^{-/-}$ MEFs were included in each qPCR run, and null and floxed allele frequencies in experimental samples were calculated relative to these standards. Primer sequences are listed in *SI Materials and Methods*.

Immunoblot Analysis. Detailed descriptions of the processing procedures used to generate tissue and WBC protein lysates for immunoblot analyses are provided in *SI Materials and Methods*. Antibodies used in immunoblot analyses were: RBP2 (Cell Signaling Technology, 3876) and vinculin (Sigma, V9131).

Mouse Experiments. All mouse procedures were approved by the Institutional Animal Care and Use Committee of the Dana-Farber Cancer Institute. All mice were housed in the animal research facility of the Dana-Farber Cancer Institute in accordance with the National Institutes of Health guidelines (26).
Breeding strategy. $Rbp2^{lox/lox}$ mice and mice harboring the *Cre–ER* transgene driven by the CAGG promoter were described previously (20, 24, 43, 44). $Rb1^{+/-}$ mice were purchased from The Jackson Laboratory. All mice were backcrossed to C57BL/6 strain for at least five generations. $Rbp2^{lox/lox}$ and *Cre–ER* mice were crossed to obtain $Rbp2^{+/lox}$; *Cre–ER* mice. These mice were crossed to $Rbp2^{+/lox}$ mice to generate $Rbp2^{lox/lox}$; *Cre–ER* mice. $Rbp2^{lox/lox}$; *Cre–ER* mice were crossed with $Rb1^{+/-}$ mice to produce $Rbp2^{+/lox}$; $Rb1^{+/-}$; *Cre–ER* progeny. These mice were mated with $Rbp2^{+/lox}$; $Rb1^{+/-}$ mice to produce $Rbp2^{lox/lox}$; $Rb1^{+/-}$; *Cre–ER* mice. Finally, *Cre–ER* mice were crossed with $Rb1^{+/-}$ mice to yield $Rbp2^{+/+}$; $Rb1^{+/-}$; *Cre–ER* mice.
High-dose tamoxifen treatments. Tamoxifen was administered at a dose of 160 mg/kg via oral gavage (4 mL/kg). For short-term studies in mice without tumors, tamoxifen was administered on 5 consecutive days. For the long-term study evaluating the impact of RBP2 suppression in $Rb1^{+/-}$ mice, tamoxifen was administered on 5 consecutive days starting at the time of tumor detection and then once per week until each mouse was euthanized due to tumor burden. Additional experimental details are provided in *SI Materials and Methods*.
Magnetic resonance imaging. MRI details are provided in *SI Materials and Methods*.
Survival analysis. $Rb1^{+/-}$ mice were monitored frequently for morbidity associated with tumor burden throughout all of the studies described. Mice were euthanized when they exhibited labored breathing, displayed symptoms of neurological distress (including poor grooming, circling, hunched posture, and others), exhibited >25% body weight loss, or became generally moribund. Pituitary and/or thyroid tumors were harvested immediately after euthanizing. Of the 24 mice in each cohort that were evaluated for tumor formation via MRI, four mice (three $Rbp2^{+/+}$ and one $Rbp2^{lox/lox}$) were not enrolled in the study and were excluded from all analyses. All four of these mice were euthanized before tamoxifen treatment commenced: three of them developed severe dermatitis, and one mouse displayed neurological abnormalities.

Histology and Immunohistochemistry. Tissues were harvested and immediately fixed for 24 h in 10% formalin in PBS. Tissues were washed with and stored in 70% ethanol before paraffin embedding. For histologic analyses of hearts and pituitary/thyroid tumors, paraffin-embedded tissues were sectioned and stained with hematoxylin and eosin (H&E). H&E-stained heart and tumor tissues were reviewed by pathologists R.T.B. and S.S., respectively. For immunohistochemistry analyses, antibodies used were: anti-RBP2 (Abcam, ab194286), anti-pRb (Abcam, ab181616), anti-SMCX (Abcam, ab190181), and anti-H3K4me3 (Cell Signaling, 9751). Additional experimental details are provided in *SI Materials and Methods*.

Statistical Analysis. Statistical analyses were carried out using GraphPad Prism software and R statistical software. *P* values for all comparisons other than those pertaining to tumor growth, survival, and gender composition of mouse cohorts were calculated by unpaired two-tailed *t* test. For comparisons of two groups with significantly different variances, Welch's *t* test was used. For comparisons of two groups without significant differences in variances, Student's *t* test was used. Differences in tumor growth kinetics

between *Rbp2*$^{+/+}$; *Rb1*$^{+/-}$; *Cre–ER* and *Rbp2*$^{lox/lox}$; *Rb1*$^{+/-}$; *Cre–ER* cohorts were analyzed with a linear mixed-effects model using the R package *nlme*. Tumors arising in mice that required euthanizing before the first posttreatment MRI could be completed and tumors that developed after tamoxifen treatment were excluded from tumor burden calculations. For the survival study, significance was determined by log-rank test. Statistical analysis of gender composition in the *Rbp2*$^{+/+}$; *Rb1*$^{+/-}$; *Cre–ER* and *Rbp2*$^{lox/lox}$; *Rb1*$^{+/-}$; *Cre–ER* cohorts was performed using Fisher's exact test. Statistical significance for all comparisons was determined using a nominal P value <0.05.

ACKNOWLEDGMENTS. We thank members of the W.G.K. and J.-A.L. laboratories at the Dana-Farber Cancer Institute for helpful discussions and the Technical Services staff of the Animal Resources Facility of Dana-Farber Cancer Institute for technical assistance. S.K.M. is supported by postdoctoral fellowship PF-14-144-01-TBE from the American Cancer Society and by a Career Enhancement Project award from the Dana-Farber/Harvard Cancer Center Brain Specialized Program of Research Excellence (SPORE). W.G.K. is a Howard Hughes Medical Institute Investigator and is supported by grants from the NIH.

1. Burkhart DL, Sage J (2008) Cellular mechanisms of tumour suppression by the retinoblastoma gene. *Nat Rev Cancer* 8:671–682.
2. Qin XQ, Chittenden T, Livingston DM, Kaelin WG, Jr (1992) Identification of a growth suppression domain within the retinoblastoma gene product. *Genes Dev* 6:953–964.
3. Binné UK, et al. (2007) Retinoblastoma protein and anaphase-promoting complex physically interact and functionally cooperate during cell-cycle exit. *Nat Cell Biol* 9: 225–232.
4. Hiebert SW, Chellappan SP, Horowitz JM, Nevins JR (1992) The interaction of RB with E2F coincides with an inhibition of the transcriptional activity of E2F. *Genes Dev* 6: 177–185.
5. Sellers WR, et al. (1998) Stable binding to E2F is not required for the retinoblastoma protein to activate transcription, promote differentiation, and suppress tumor cell growth. *Genes Dev* 12:95–106.
6. Miyake S, et al. (2000) Cells degrade a novel inhibitor of differentiation with E1A-like properties upon exiting the cell cycle. *Mol Cell Biol* 20:8889–8902.
7. Gu W, et al. (1993) Interaction of myogenic factors and the retinoblastoma protein mediates muscle cell commitment and differentiation. *Cell* 72:309–324.
8. Chen PL, Riley DJ, Chen Y, Lee WH (1996) Retinoblastoma protein positively regulates terminal adipocyte differentiation through direct interaction with C/EBPs. *Genes Dev* 10:2794–2804.
9. Talluri S, et al. (2010) A G1 checkpoint mediated by the retinoblastoma protein that is dispensable in terminal differentiation but essential for senescence. *Mol Cell Biol* 30: 948–960.
10. Chicas A, et al. (2010) Dissecting the unique role of the retinoblastoma tumor suppressor during cellular senescence. *Cancer Cell* 17:376–387.
11. Adams PD, et al. (1999) Retinoblastoma protein contains a C-terminal motif that targets it for phosphorylation by cyclin-cdk complexes. *Mol Cell Biol* 19:1068–1080.
12. George J, et al. (2015) Comprehensive genomic profiles of small cell lung cancer. *Nature* 524:47–53.
13. Oser MG, Niederst MJ, Sequist LV, Engelman JA (2015) Transformation from non-small-cell lung cancer to small-cell lung cancer: Molecular drivers and cells of origin. *Lancet Oncol* 16:e165–e172.
14. Niederst MJ, et al. (2015) RB loss in resistant EGFR mutant lung adenocarcinomas that transform to small-cell lung cancer. *Nat Commun* 6:6377.
15. Sequist LV, et al. (2011) Genotypic and histological evolution of lung cancers acquiring resistance to EGFR inhibitors. *Sci Transl Med* 3:75ra26.
16. Tan HL, et al. (2014) Rb loss is characteristic of prostatic small cell neuroendocrine carcinoma. *Clin Cancer Res* 20:890–903.
17. Hu N, et al. (1994) Heterozygous Rb-1 delta 20/+mice are predisposed to tumors of the pituitary gland with a nearly complete penetrance. *Oncogene* 9:1021–1027.
18. Jacks T, et al. (1992) Effects of an Rb mutation in the mouse. *Nature* 359:295–300.
19. Benevolenskaya EV, Murray HL, Branton P, Young RA, Kaelin WG, Jr (2005) Binding of pRB to the PHD protein RBP2 promotes cellular differentiation. *Mol Cell* 18:623–635.
20. Lin W, et al. (2011) Loss of the retinoblastoma binding protein 2 (RBP2) histone demethylase suppresses tumorigenesis in mice lacking Rb1 or Men1. *Proc Natl Acad Sci USA* 108:13379–13386.
21. Cao J, et al. (2014) Histone demethylase RBP2 is critical for breast cancer progression and metastasis. *Cell Rep* 6:868–877.
22. Teng YC, et al. (2013) Histone demethylase RBP2 promotes lung tumorigenesis and cancer metastasis. *Cancer Res* 73:4711–4721.
23. Sharma SV, et al. (2010) A chromatin-mediated reversible drug-tolerant state in cancer cell subpopulations. *Cell* 141:69–80.
24. Klose RJ, et al. (2007) The retinoblastoma binding protein RBP2 is an H3K4 demethylase. *Cell* 128:889–900.
25. Zaidi S, et al. (2013) De novo mutations in histone-modifying genes in congenital heart disease. *Nature* 498:220–223.
26. National Research Council (2011) *Guide for the Care and Use of Laboratory Animals* (National Academies Press, Washington, DC), 8th Ed.
27. Maggi EC, et al. (2016) Retinoblastoma-binding protein 2 (RBP2) is frequently expressed in neuroendocrine tumors and promotes the neoplastic phenotype. *Oncogenesis* 5:e257.
28. Zeng J, et al. (2010) The histone demethylase RBP2 Is overexpressed in gastric cancer and its inhibition triggers senescence of cancer cells. *Gastroenterology* 138:981–992.
29. Defeo-Jones D, et al. (1991) Cloning of cDNAs for cellular proteins that bind to the retinoblastoma gene product. *Nature* 352:251–254.
30. Kim YW, Otterson GA, Kratzke RA, Coxon AB, Kaye FJ (1994) Differential specificity for binding of retinoblastoma binding protein 2 to RB, p107, and TATA-binding protein. *Mol Cell Biol* 14:7256–7264.
31. Fattaey AR, et al. (1993) Characterization of the retinoblastoma binding proteins RBP1 and RBP2. *Oncogene* 8:3149–3156.
32. Gale M, et al. (2016) Screen-identified selective inhibitor of lysine demethylase 5A blocks cancer cell growth and drug resistance. *Oncotarget* 7:39931–39944.
33. Vinogradova M, et al. (2016) An inhibitor of KDM5 demethylases reduces survival of drug-tolerant cancer cells. *Nat Chem Biol* 12:531–538.
34. Gehling VS, et al. (2016) Identification of potent, selective KDM5 inhibitors. *Bioorg Med Chem Lett* 26:4350–4354.
35. Labadie SS, et al. (2016) Design and evaluation of 1,7-naphthyridones as novel KDM5 inhibitors. *Bioorg Med Chem Lett* 26:4492–4496.
36. Westaway SM, et al. (2016) Cell penetrant inhibitors of the KDM4 and KDM5 families of histone lysine demethylases. 1. 3-amino-4-pyridine carboxylate derivatives. *J Med Chem* 59:1357–1369.
37. Westaway SM, et al. (2016) Cell penetrant inhibitors of the KDM4 and KDM5 families of histone lysine demethylases. 2. Pyrido[3,4-d]pyrimidin-4(3H)-one derivatives. *J Med Chem* 59:1370–1387.
38. Horton JR, et al. (2016) Structural basis for KDM5A histone lysine demethylase inhibition by diverse compounds. *Cell Chem Biol* 23:769–781.
39. Bavetsias V, et al. (2016) 8-substituted pyrido[3,4-d]pyrimidin-4(3H)-one derivatives as potent, cell permeable, KDM4 (JMJD2) and KDM5 (JARID1) histone lysine demethylase inhibitors. *J Med Chem* 59:1388–1409.
40. Wang L, et al. (2013) A small molecule modulates Jumonji histone demethylase activity and selectively inhibits cancer growth. *Nat Commun* 4:2035.
41. Roesch A, et al. (2010) A temporarily distinct subpopulation of slow-cycling melanoma cells is required for continuous tumor growth. *Cell* 141:583–594.
42. Roesch A, et al. (2013) Overcoming intrinsic multidrug resistance in melanoma by blocking the mitochondrial respiratory chain of slow-cycling JARID1B(high) cells. *Cancer Cell* 23:811–825.
43. Minamishima YA, et al. (2008) Somatic inactivation of the PHD2 prolyl hydroxylase causes polycythemia and congestive heart failure. *Blood* 111:3236–3244.
44. Hayashi S, McMahon AP (2002) Efficient recombination in diverse tissues by a tamoxifen-inducible form of Cre: A tool for temporally regulated gene activation/inactivation in the mouse. *Dev Biol* 244:305–318.